Progress In Electromagnetics Research, Vol. 128, 419–440, 2012

AN ACTIVE RING SLOT WITH RF MEMS SWITCHABLE RADIAL STUBS FOR RECONFIGURABLE FREQUENCY SELECTIVE SURFACE APPLICATIONS

R. Martinez-Lopez, J. Rodriguez-Cuevas, A. E. Martynyuk, and J. I. Martinez-Lopez*

Faculty of Engineering, National Autonomous University of Mexico (UNAM), Mexico D.F., Mexico

Abstract—An active ring slot resonator loaded by switchable radial stubs is investigated. It is shown that this element can be used as the unit cell of a switchable reconfigurable frequency selective surface (RFSS). Equivalent circuit and full-wave mathematical models are obtained to evaluate the reflection characteristics of the RFSS based on this element. The possibility to obtain different resonant transmission frequencies is discussed. The mathematical model developed is used to design an X band RFSS capable of obtaining resonant frequencies at 9.65, 10.28, 10.83 and 12.05 GHz. Commercially available RF MEMS switches are used to evaluate the effect of the off-state capacitances over the response of the periodic structure. To validate the numerical simulation results, different active and passive diaphragms were designed, fabricated, and tested using the waveguide simulator. A good agreement between numerical and measured results was found.

1. INTRODUCTION

Saturation of the radio electric spectrum due to the high demands on wireless data transmission has led the communication industry to implement various electromagnetic compatibility techniques to make the communication process more efficient and safe. These techniques are intended to overcome the challenges of receiving weak radio waves that suffer from strong interference in local environments overwhelmed with electromagnetic signals. Communication systems can benefit from frequency selective surfaces (FSS) with the ability to filter the incoming signals in the frequency domain [1, 2]. Frequency

Received 12 April 2012, Accepted 18 May 2012, Scheduled 2 June 2012

* Corresponding author: Jose I. Martinez Lopez (ismartz@servidor.unam.mx).

diversity and polarization diversity schemes provided by the FSS can diminish the unwanted interference. FSS has become useful in wireless high frequency communication systems due to the following reasons: a) the enhancement of the spectral efficiency when the interference produced by neighboring antennas operating on nearby frequencies is blocked [3], b) the improvement of the antenna's radiation characteristics [4–6], c) the improvement of the security in wireless indoor communication networks through binding typically unbound signals [7], and d) the circumvention of difficulties in obtaining low-loss lumped-element components needed for high quality tuning circuits [8]. Besides the conventional applications of FSS in filters, polarizers, subreflectors, and radomes, recent applications of FSS include artificial magnetic conductors [9–12], electromagnetic bandgap materials [13, 14], superstrate antenna arrays [15], metamaterials [16], and electromagnetic architecture of buildings [17]. Furthermore, active or reconfigurable frequency selective surfaces (RFSS) have become attractive due to their capability to dynamically change their resonant frequencies [18, 19]. This flexibility allows the RFSS to be utilized in various applications, particularly when the surrounding environment is both complex and dynamic, and the adjustment of the resonant frequencies needs to be achieved rapidly.

Different methods have been used to reconfigure or tune the response of the RFSS: a) by modifying the constitutive parameters of the FSS screen or substrate [20–23], b) by changing the geometry of the periodic unit cell [24], and c) by introducing control devices into the periodic unit cell [25, 26]. In fact, active control devices at microwave frequencies are able to ensure a rapid response in the RFSS's elements. Generally, these active devices such as pin diodes, varactor diodes, and RF MEMS have been used to obtain a fast reconfiguration of the RFSS's resonant frequency [27–30]. However, at high frequencies, control devices with low insertion loss and negligible parasitics are difficult to find. These issues can become a substantial problem in the overall performance of the RFSS. Generally, non-ideal aspects of control devices affect the RFSS characteristics as well as its performance. For example, pin diodes demand a large control power, which is particularly problematic in RFSS applications because a fabricated medium-size array will contain hundreds of these diodes. On a similar vein, the impedance of the varactor diode is easily controlled by a DC voltage, however varactors have high insertion loss levels, particularly at low-reverse bias voltages. On the other hand, RF MEMS switches are poised as the technology capable of supplying the two key characteristics of low control power and low insertion loss in the design of RFSSs. Furthermore, it is possible to monolithically integrate

MEMS devices on microwave friendly substrates to reduce insertion loss. Indeed, for this reason, monolithically integrated MEMS switches have been used to build RFSSs [31, 32] or periodic arrays [33, 34]. However, due to the non-standard fabrication processes used in MEMS technology, these devices have only been utilized in customized designs. In this paper, the potential of building a RFSS based on commercially available RF MEMS switches is explored.

In the design of FSS, different geometries of the unit cell have been used. Of these geometries, ring based designs have shown excellent performance in supporting various types of polarizations and have demonstrated a good insensibility with respect to the angle of incidence [35]. Various FSS and RFSS based on rings have been proposed, including shorted ring slots, loaded ring slots, active rings, split rings, and trapped rings [36–39]. Furthermore, ring slot FSSs have demonstrated low insertion loss and low cross-polarization levels [40]. In this work, a ring slot resonator loaded with switchable radial stubs for applications in RFSS is investigated. The appropriate switching of the stubs provides the electronic control of the RFSS's main characteristics, ensuring different transmission resonant frequencies with a defined reconfigurability range as well as polarization diversity.

2. PRINCIPLE OF OPERATION

The geometry of the proposed RFSS element is shown in Fig. 1(a). This element contains a ring slot resonator with eight switchable and eight non-switchable inductive radial stubs connected to the outer part of the ring slot. The angle between any two adjacent switchable stubs as well as the angle between any two adjacent non-switchable stubs is 45°. As the switchable and non-switchable stubs are alternated, the angle between any pair of adjacent stubs is 22.5°. The inner and outer radii of the ring slot are r_1 and r_2, respectively. The non-switchable stubs (u_1, u_2, u_3, ..., u_8) have a length of l_f. The switchable radial stubs (t_1, t_2, t_3, ..., t_8) are of two lengths, the first ones (t_1, t_3, t_5, and t_7) have lengths of l_s, and the second ones (t_2, t_4, t_6, and t_8) have a longer length of l_l. While the lengths of the stubs vary, both switchable and non-switchable stubs have the same width of w. Eight switches (s_1, s_2, s_3, ..., s_8) are respectively connected in parallel to the switchable radial stubs as it is shown in Fig. 1(a). This RFSS element is printed on a dielectric substrate with relative dielectric permittivity of ε_r and dielectric thickness of h_r. The related RFSS shown in Fig. 1(b) contains multiple elements arranged at the nodes of a rectangular grid with periodicity b_x and b_y along the x- and y-directions, respectively.

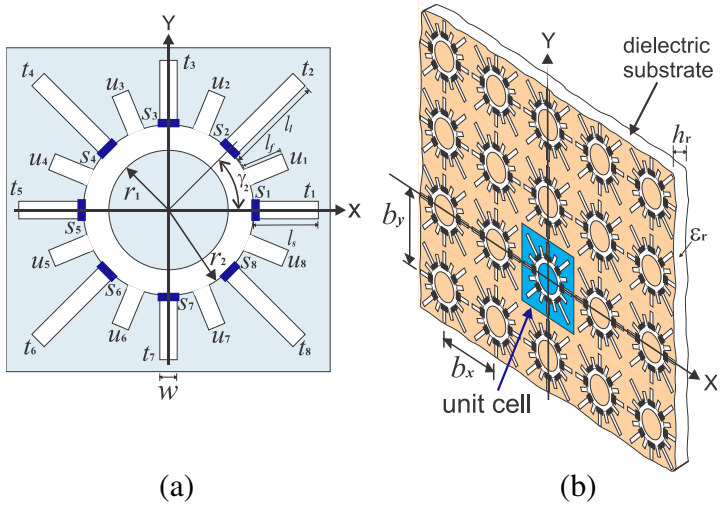

Figure 1. RFSS based on ring slot with switchable radial stubs. (a) Geometry of the unit cell. (b) Periodic grid of the RFSS.

The key characteristic of the above mentioned RFSS element is the resonant behavior of its reflection coefficient. The reconfiguration of its reflection characteristics is achieved by loading the ring slot with switchable radial stubs. The off- or on-state of a switch allows the corresponding switchable stub to be connected or disconnected to the ring, respectively. Now, in order to justify the presence of the non-switchable radial stubs, consider the following example: suppose that the maximum reconfigurable frequency of the RFSS corresponds to a free-space wavelength $\lambda_{0_{\min}}$. In this case, all the switchable stubs need to be disconnected to achieve the highest resonant frequency for the ring slot. To avoid grating lobes in square lattice arrays for the case of oblique incidence, the spacing between adjacent elements must not exceed $\lambda_{0_{\min}}/2$. Thus, the minimum diameter of the ring slot is approximately equal to $\lambda_{0_{\min}}/3$, allowing a maximum distance of approximately $\lambda_{0_{\min}}/15$ between the outer part of the ring and the edge of the unit cell. This remaining space is allocated to the switchable stubs. As the reconfigurability range of the RFSS depends on the frequency shift produced by loading the ring, and this loading depends on the length of the stubs, the aforementioned space is too small for stubs able to extend the reconfigurability range. One way to reduce the diameter of the ring slot is by using substrate loading, however, dielectric losses and the presence of surface waves can be expensive consequences when using thick, high permeability

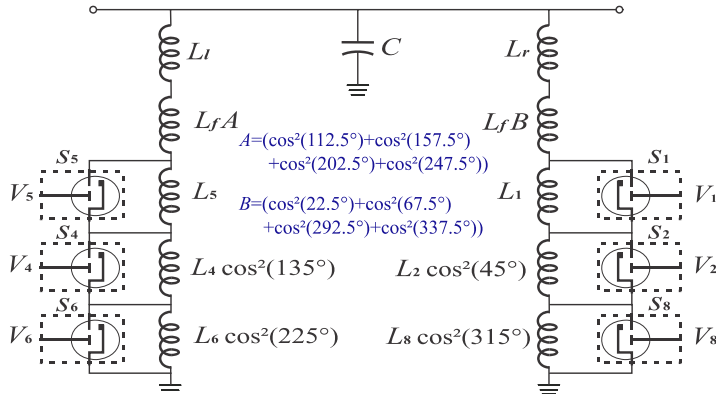

Figure 2. Equivalent circuit model of the RFSS element in the case of y-polarization.

substrates. Therefore, the usage of non-switchable stubs that reduce the resonant frequencies of the element is an adequate solution for the miniaturization of the unit cell. Furthermore, the non-switchable stubs introduce a degree of freedom that provides more flexibility in the design of the RFSS.

In order to explain the operation principle of the RFSS element, an equivalent circuit model of the element is proposed. The model for the case of a y-polarized normally incident wave is shown in Fig. 2. The capacitance C and the inductances L_l and L_r form the equivalent circuit of the ring slot resonator. The capacitance C is due to the electrical field stored in the ring slot, and the inductances L_l and L_r are due to the currents that flow on the outer left and right parts of the metal, respectively. L_f is the inductance for each of the non-switchable stubs, meanwhile L_k is the inductance corresponding to the k-th switchable stub (for $k = 1, \ldots, 8$). V_k is the control voltage to toggle the k-th switch. The excitation of the stubs and the currents that flow across the switches depend on the polarization of the incident wave. To account for this dependence, the trigonometric function $\cos^2(\gamma_k)$ is used, where γ_k is angular position of the k-th stub with respect to the x axis.

Now, consider the effects of the commutation of the switches in the RFSS element. When all the switches are in the off-state, the element behaves as a ring slot resonator loaded by all the stubs and the minimum resonant frequency $\omega_{\min}$ is obtained due to the maximum loading of the ring slot. It is important to notice that when a square lattice is used, the switchable stubs located at the

corners of the unit cell have longer lengths to extend the loading of the ring. On the other hand, when all the switches are in the on-state, all the switchable stubs are disconnected and the element behaves as an unloaded ring slot resonator loaded only by the non-switchable stubs. This condition provides the maximum resonant frequency $\omega_{\max}$. Consequently, different on-off combinations for the switches allow the ring to have different loading conditions and thus different resonant frequencies between $\omega_{\min}$ and $\omega_{\max}$.

The proposed RFSS element offers the flexibility to provide polarization diversity. Certain on-off configurations of the switches are suitable for circular polarizations, while others fit better with linear polarizations. For circular polarization applications, an equal loading for both x and y components of the incident wave is needed. For linear polarization applications, symmetry with respect to the axis parallel to the electric field vector of the incident wave is required.

3. MATHEMATICAL MODEL

Analysis and optimization of switchable RFSS require multiple simulations of the same geometry for different on-off configurations of the switches. Generally, commercial full-wave simulators require a complete recalculation of the RFSS even in the case when only one of the switches changes its state. Thus, it is highly desirable to develop a full-wave mathematical model that allows a fast recalculation of the reflection characteristics of the RFSS for a new set of switch states. Therefore, a special full-wave mathematical model based on the Method of Moments (MoM) was developed to analyze the proposed switchable RFSS [41, 42]. The RFSS is treated as an infinite periodic structure with a periodic cell that contains differently-configured switches. According to Floquet's theorem, the reflected and transmitted electromagnetic fields of the infinite FSSs can be presented as a summation of plane waves (or Floquet modes). Thus, the unknown electric field distribution on both sides of the aperture is expanded into a set of Floquet modal functions. Also, these modes in conjunction with their corresponding modal admittances are used to express the unknown magnetic field on both sides of the surface. By matching these tangential field components at the plane of the RFSS, one can obtain an integral equation for the unknown electric field. In order to allow the fast recalculation of the same RFSS for the different states of the switching elements, the unknown tangential electric field at the plane of the RFSS is presented as a sum of two components:

$$\vec{E}_\tau = \vec{E}_\tau^u + \vec{E}_\tau^I \tag{1}$$

The first component $\vec{E}_\tau^u$ is the tangential electric field that appears considering that the incident plane wave excites the RFSS element without switches. The second component is the tangential electric field $\vec{E}_\tau^I$ that appears due to the electric currents I_k that flow across the switches. According to (1), the calculation of the $\vec{E}_\tau^u$ is performed once and then only the $\vec{E}_\tau^I$ is recalculated for the different states of the switches.

The Fredholm integral equation with respect to the unknown $\vec{E}_\tau^u$ can be obtained by applying both the boundary conditions for the tangential electric field and the continuity condition for the tangential magnetic field over the aperture:

$$2A_0Y_0\vec{\Psi}_0(x,y)=\sum_{n=1}^{\infty}\left(Y_n+Y_n^d\right)\vec{\Psi}_n(x,y)\iint_{A'}\vec{E}_\tau^u(x,y)\cdot\vec{\Psi}_n^*(x,y)dxdy, \quad (2)$$

where $\vec{\Psi}_n(x, y)$ is the complete set of Floquet modes of the unit cell, Y_n is the admittance of the corresponding Floquet mode $\vec{\Psi}_n$, Y_n^d is the modified admittance of the corresponding Floquet mode $\vec{\Psi}_n$ that takes into account the dielectric substrate [43], A_0 and Y_0 are the magnitude and the admittance of the incident Floquet mode $\vec{\Psi}_0(x, y)$, respectively, A' is the aperture area of the unit cell, and the symbol * denotes the complex conjugation. This equation is solved to obtain $\vec{E}_\tau^u$ using the MoM in Galerkin's form. Eigenfunctions of the coaxial waveguide with stubs were used as the basis and weighting functions.

The integral equation with respect to the unknown $\vec{E}_\tau^I$ can be obtained by applying the continuity condition for the tangential magnetic field across the surface of the aperture including the switches. It is important to point out that the magnetic field is not continuous in the regions where the currents flow across the switches. Therefore, the electric currents must be considered in the following integral equation:

$$\sum_{n=1}^{\infty}\left(Y_n+Y_n^d\right)\vec{\Psi}_n(x,y)\iint_{A'}\vec{E}_\tau^I\cdot\vec{\Psi}_n^*(x,y)dxdy=-\sum_{k=1}^{K}I_k\vec{P}_k(\rho,\varphi) \quad (3)$$

where I_k is the electric current across the switch k, and K is the total number of switches in the unit cell. $\vec{P}_k(\rho, \varphi)$ is the vector function that converts the electric current I_k into the corresponding current density.

If the dimensions of the switch are negligible with respect to the wavelength, one can consider that:

a) The geometry of the switch can be approximated by a circular trapezoid defined by an angular size $\Delta\varphi = w/r_2$, and radii r_2

and $r_2 + w_s$, where w_s is the width of the switch. The function $\vec{P}_k(\rho, \varphi)$ can be expressed in the following form:

$$\vec{P}_k(\rho,\varphi)=\vec{a}_\varphi[1(r_2+w_s)-1(r_2)] \times\left[1\left(\varphi_{0k}+\frac{\Delta\varphi}{2}\right)-1\left(\varphi_{0k}-\frac{\Delta\varphi}{2}\right)\right]/w_s, \text{ for, } k=1,\ldots,K, \quad (4)$$

where $\vec{a}_\varphi$ is the unit vector in φ direction, φ_{0k} is the center's angular position of the k-th switch, and $1(x)$ is the Heaviside unit step function.

b) Ohm's law can be applied to obtain the additional equations for the unknown currents I_k:

$$\int_P \left(\vec{E}_\tau^u + \vec{E}_\tau^I\right) \cdot d\vec{l} = I_k \bar{Z}_k, \quad \text{for,} \quad k = 1,\ldots,K, \quad (5)$$

where P is the line path where I_k exists and $\bar{Z}_k$ is the corresponding impedance of the k-th switch.

The system of integral Equations (3), (5) can be then reduced to a system of linear equations using the Galerkin's MoM and solved simultaneously to calculate $\vec{E}_\tau^I$. When the field distributions of $\vec{E}_\tau^u$ and $\vec{E}_\tau^I$ are calculated, one can evaluate the electromagnetic fields in front of and behind the RFSS, and then obtain the reflection characteristics of the array. Note that according to the presented mathematical model only the right part in (5) changes when the switches in the RFSS are commutated.

4. SIMULATED PERFORMANCE OF THE RFSS BASED ON THE RECONFIGURABLE ELEMENT

4.1. RFSS with Metal Strips and Open Circuits Instead of Switching Elements

To demonstrate the suitability of the proposed element for RFSS applications, the reflection characteristics of an infinite array were simulated using the above mentioned mathematical model. At first RFSS with metal strips and ideal open circuits, instead of switching elements, were analyzed. Two geometries of the element were investigated. Geometry I is given by: $r_1 = 2.2\,\text{mm}$, $r_2 = 2.8\,\text{mm}$, $l_f = 1.8\,\text{mm}$, $l_s = 2.1\,\text{mm}$, $l_l = 3.7\,\text{mm}$, $w = 0.6\,\text{mm}$, and $b_x = b_y = 11.43\,\text{mm}$. Geometry II is given by: $r_1 = 3\,\text{mm}$, $r_2 = 3.5\,\text{mm}$, $l_f = 0.3\,\text{mm}$, $l_s = 1.4\,\text{mm}$, $l_l = 2.3\,\text{mm}$, $w = 0.6\,\text{mm}$, and $b_x = b_y = 11.43\,\text{mm}$. In these simulations, it was assumed that the elements were printed on a dielectric substrate of $\varepsilon_r = 3.4$ and $h_r = 0.51\,\text{mm}$.

On-states of the switches were simulated with metal strips of $w_s = 0.2$ mm, while off-states were considered as open circuits. Basically, these descriptions mean that Geometry I contains a smaller ring slot circumference with longer stubs, while Geometry II contains a larger ring slot circumference with shorter stubs.

To evaluate the reconfigurability of the proposed RFSS element, four different on-off configurations (1, 2, 3, 4) of the switches were investigated. The scattering of the y-polarized normally incident wave over an infinite RFSS was simulated. In the case of Configuration 1, all the switches are in the off-state. Thus, the maximum loading of the ring slot is obtained, producing the lowest resonant frequency. Configuration 2 with switches s_1, s_3, s_5, and s_7 in the on-state provides the second lowest resonant frequency, due to the loading of the ring slot by fixed stubs and stubs t_2, t_4, t_6 and t_8. Configuration 3 with switches s_2, s_4, s_6, and s_8 in the on-state allows the ring to have the loading from the non-switchable stubs and stubs t_1 and t_5, in this case the resonant frequency is higher than in the previous case. Finally, Configuration 4 with all switches in the on-state provides the highest resonant frequency due to the loading of the ring slot only from the non-switchable stubs. The simulated results for Geometries I and II are presented in Figs. 3(a) and 3(b), respectively.

From the previous results, one can observe that the RFSS is able to reconfigure four resonant transmission frequencies. Geometry I sets the resonant frequencies of 9.48, 9.80, 10.85, and 11.83 GHz for

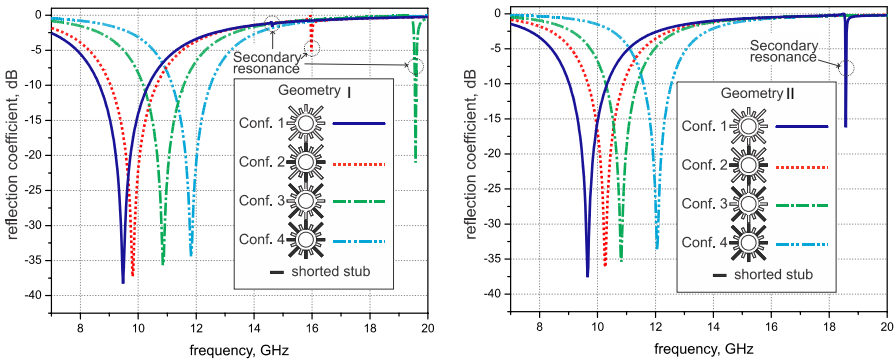

Figure 3. Simulated reflection coefficient of the infinite RFSS with metal strips and open circuits instead of switching elements in the case of a y-polarized normally incident wave. (a) Geometry I. (b) Geometry II.

Configurations 1, 2, 3, and 4, respectively, meanwhile Geometry II sets 9.65, 10.28, 10.83, and 12.05 GHz for Configurations 1, 2, 3, and 4, respectively. The secondary resonances for Configuration 1 appear at 14.63 and 18.58 GHz for Geometries I and II, respectively. Geometry I shows the appearance of undesirable secondary resonances at lower frequencies than Geometry II. As the on- and off-states of the switches are simulated by metal strips and open circuits, respectively, these secondary resonances can only be explained by the resonant characteristics of short-ended stubs, as longer stubs have lower resonant frequencies than shorter stubs.

4.2. Effect of the Switch's Impedances on the RFSS Performance

In the performance of switchable RFSS, the main effects from switch parasitics are the dissipative loss and the resonance frequency shift. Dissipative loss of the RFSS strongly depends on the commutation quality factor of the switch [44], while the frequency shift is due to the loading of the switch's off-state capacitance. Minimization of dissipative loss can be accomplished by optimal transformation of switch impedances [45]. As the lower frequencies of the RFSS are obtained by loading the ring slot, the effect of this capacitive loading can be used to downward shifts of the resonance transmission frequencies and thus extend the reconfigurability range of the RFSS. This improvement is repeatable due to the narrow spread in the values of the RF MEMS switch's off-state capacitance. However, the connection of the switch's off-state capacitance in parallel to the inductive stubs causes an anti-resonance followed by a secondary resonance that can reduce the upper stop band of the RFSS.

To evaluate the effect of the switch's off-state impedance for different lengths of the stubs, the reflection coefficients for Geometries I and II were simulated. A parallel connection of a capacitance C_{OFF} and a resistance R_{OFF} was used as the model of the off-state switch's impedance. For both geometries, the parameters of a typical switch were set to $C_{\mathrm{OFF}} = 0.056\,\mathrm{pF}$ and $R_{\mathrm{OFF}} = 3\,\mathrm{k}\Omega$. Figs. 4(a) and 4(b) shows the calculated reflection coefficients of the RFSS along with the above mentioned model. The resonant frequencies for Geometry I are 8.15, 8.28, 10.03, and 11.83 GHz for Configurations 1, 2, 3 and 4, respectively, while the resonant frequencies for Geometry II are 8.88, 9.30, 10.23, and 12.05 GHz for Configurations 1, 2, 3 and 4, respectively. For Geometry I, the secondary resonances are 10.60, 13.38, and 14.48 GHz for Configurations 1, 2, and 3, respectively, while for Geometry II, the secondary resonances are 12.78, 15.75, and 17.33 GHz for Configurations 1, 2, and 3, respectively. When these

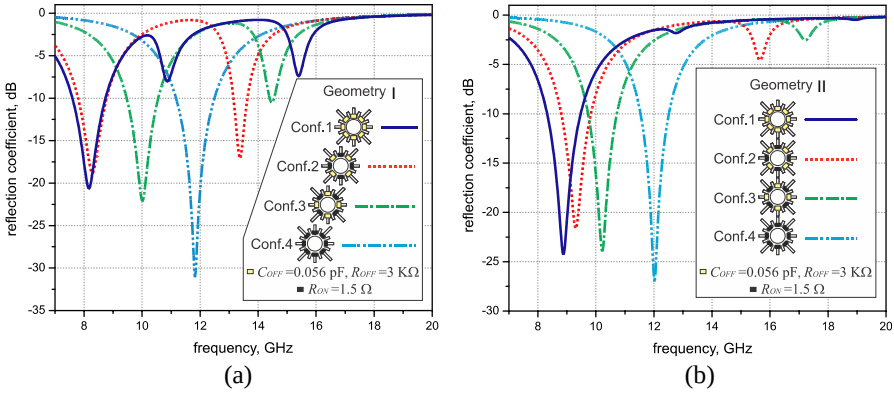

Figure 4. Simulated reflection coefficients for infinite RFSS with switching elements in the case of a y-polarized normally incident wave. (a) Geometry I. (b) Geometry II.

results are compared with the cases using metal strips and open circuits instead of switching elements described in Section 4.1, a downward frequency shift in the main resonance and the onset of unwanted secondary resonances are observed. Thus, it is observed an increase in the reconfigurability range of 56.6% and 32.1% for Geometry I and Geometry II, respectively. On the other hand, Geometry II, containing shorter stubs, has less sensitivity to the onset of secondary resonances when compared with Geometry I.

To evaluate the effect of the off-state switch's impedance on the RFSS element's performance for different widths of the ring slot, a particular case of one ring slot loaded with only two horizontal switchable radial stubs t_1 and t_2 was analyzed (Fig. 5(a)). This particular geometry evaluates the interaction of the ring slot and the switchable stubs in the case that the element is illuminated by a y-polarization incident wave. The equivalent electrical circuit model for the case of the off-state switches is depicted in Fig. 5(b). Inductances L_l and L_r are due to the currents that flow on the outer left and right parts of the metal, respectively, and L_s is the inductance of the radial stub. Due to the element's symmetry, L_l and L_r are equal.

According to the equivalent circuit model, the resonant frequencies $(\omega_1, \ldots, \omega_4)$ can be estimated by obtaining the roots of the following admittance equation: $0.5L_rCC_{\mathrm{OFF}}L_s(j\omega)^4 + (C_{\mathrm{OFF}}L_s + 0.5C(L_r + L_s))(j\omega)^2 + 1 = 0$, where $j = \sqrt{-1}$. This equation is satisfied by two positive values of ω. These values correspond to the main and secondary resonances of the RFSS element. By maximizing the

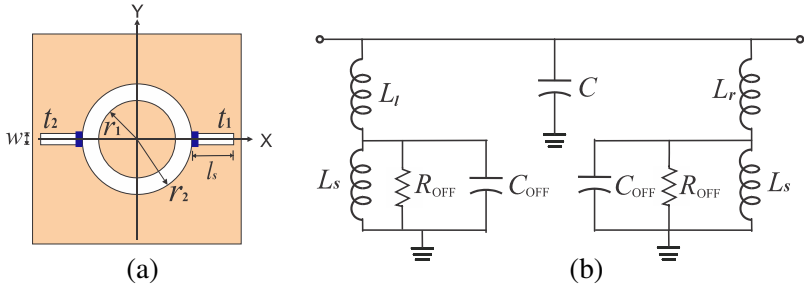

Figure 5. Ring slot loaded with two horizontal stubs. (a) Geometry of the unit cell. (b) Equivalent circuit model in the case of a y-polarized normally incident wave.

difference between these two resonances ($\Delta\omega$), the unwanted effect of the secondary resonance is minimized. In order to obtain a practical expression for this difference, one can consider, based on the typical values of the circuit elements, that L_r is larger than L_s and that C_{OFF} is larger than C. Thus $\Delta\omega$ can be approximately expressed as $\Delta\omega = 1/\sqrt{L_s C_{\text{OFF}}} - 2/\sqrt{2L_r C}$. One can observe that for given values of C_{OFF} and L_r, $\Delta\omega$ is maximized by having small values of L_s and large values of C. Therefore, RFSS elements with shorter inductive stubs and smaller slot widths are less sensitive to the switch's off-state parasitics. Additionally, the anti-resonant frequency ω_a is estimated by $\omega_a = 1/\sqrt{C_{\text{OFF}} L_s L_r/(L_s + L_r)}$.

Three different geometries (III, IV, and V) of the RFSS were evaluated using the developed mathematical model. Geometry III is given by: $r_1 = 3\,\text{mm}$, $r_2 = 3.5\,\text{mm}$; Geometry IV is set by: $r_1 = 2.75\,\text{mm}$, $r_2 = 3.75\,\text{mm}$; and Geometry V is defined as: $r_1 = 2.5\,\text{mm}$, $r_2 = 4\,\text{mm}$; and for all geometries $l_s = 1.4\,\text{mm}$ and $w = 0.6\,\text{mm}$. These unit cells are arranged at the nodes of a rectangular grid with inter-element spacings of $b_x = 11.43\,\text{mm}$ and $b_y = 10.16\,\text{mm}$ along the x- and y-directions, respectively. It was considered that the elements are printed on a dielectric substrate of $\varepsilon_r = 3.4$ and $h_r = 0.51\,\text{mm}$. For all these geometries, the parameters of the switch's off-state are $C_{\text{OFF}} = 0.056\,\text{pF}$ and $R_{\text{OFF}} = 3\,\text{k}\Omega$. Fig. 6 shows the calculated reflection coefficients for the different geometries with open circuits and with switches in the off-state.

Geometries III, IV and V with open circuits present resonant frequencies at 11.05, 12.08, and 12.70 GHz, respectively, meanwhile Geometries III, IV and V with switches show resonant frequencies at 10.35, 11.18, and 11.30 GHz. The appearance of the secondary resonances at 17.63, 17.20 and 16.50 GHz is noticed for Geometries

III, IV and V with switches in the off-state, respectively. The effects of dissipative loss, resonant frequency shifts, and the appearance of a secondary resonance are observed in the case of the Geometries with switches. It is noticed that small slot width offer the highest insensibility to the switch's off-state parasitics.

5. EXPERIMENTAL RESULTS

For validation of numerical results, the waveguide simulator was used to evaluate the performance of the proposed RFSS element. The scattering of the TE_{10} waveguide mode in the waveguide simulator corresponds to the scattering of two TE incident plane waves (two TE Floquet modes) on the infinite RFSS with an angle of incidence $\theta_0 = \sin^{-1}(\lambda/4b_x)$. Thus, different active and passive diaphragms were fabricated to be installed at the cross-section of a standard rectangular waveguide. The experimental setup was designed in two steps. The first one was designed to verify the reconfiguration capability of the RFSS. To simplify the diaphragms fabrication, metal strips were used to implement the on-states, while open circuits were used to implement the off-states. Thus, for each geometry, four diaphragms with static configurations of the on-off combinations of the switches were fabricated. The second step analyzes the behavior of the RFSS element taking into account that the switching function is accomplished by commercially available RF MEMS switches.

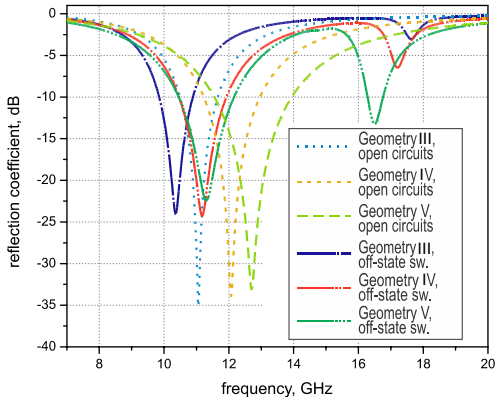

Figure 6. Simulated reflection coefficients of three different geometries with switches in the off-state and without switches.

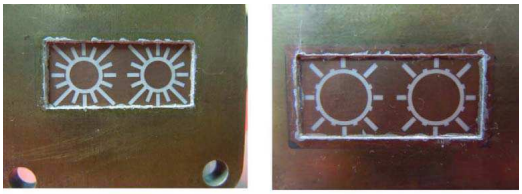

(a) (b)

Figure 7. Two-unit cell diaphragms installed at the waveguide simulator. (a) Diaphragm II (Geometry I configuration 2). (b) Diaphragm VIII (Geometry II configuration 4).

5.1. Passive Two-cell Diaphragms with Metal Strips As On-states and Open Circuits As Off-states

A total of eight two-unit cell diaphragms (I, II, ..., VIII) with metal strips as on-states and open circuits as off-states were printed on a 0.51 mm-thick 4003 Rogers substrate using a standard photolithography etching process. These diaphragms correspond to the four static configurations described in Section 4.1. Diaphragm I is given by: $r_1 = 2.2\,\text{mm}$, $r_2 = 2.8\,\text{mm}$, $l_f = 1.8\,\text{mm}$, $l_s = 2.1\,\text{mm}$, $l_l = 3.7\,\text{mm}$, $w = 0.6\,\text{mm}$, $b_x = 11.43\,\text{mm}$, and $b_y = 10.16\,\text{mm}$; and Diaphragm II is given by: $r_1 = 3\,\text{mm}$, $r_2 = 3.5\,\text{mm}$, $l_f = 0.3\,\text{mm}$, $l_s = 1.4\,\text{mm}$, $l_l = 2.3\,\text{mm}$, $w = 0.6\,\text{mm}$, $b_x = 11.43\,\text{mm}$, and $b_y = 10.16\,\text{mm}$. Fig. 7(a) shows the fabricated Diaphragm II corresponding to configuration 2 of Geometry I and Fig. 7(b) shows the fabricated Diaphragm VIII corresponding to configuration 4 of Geometry II.

These diaphragms were installed at the cross section of a rectangular waveguide WR-90. The measured reflection coefficient of the fabricated diaphragms for Geometry I and Geometry II are shown in Figs. 8(a) and (b), respectively. Additionally, the simulated reflection coefficients of the RFSS for the different configurations are shown in these same figures for comparison. Table 1 shows a summary of the measured and simulated results. Good agreement between calculated and measured results was observed.

To evaluate the efficiency of the proposed mathematical model, the calculation of the reflection coefficient (Fig. 8(a), configuration 3) was performed from 7 to 13 GHz with standard time domain and frequency domain solvers. The CPU time (Intel Core i7 960 3.2 GHz, 16 GB RAM) was 7 min 30 s for the time domain solver and 57 min 13 s for the frequency domain solver. The CPU time used for the code based on the developed mathematical model was 23 min 13 s for the first calculation, and 19 s for the subsequent recalculations when only the switch states were modified.

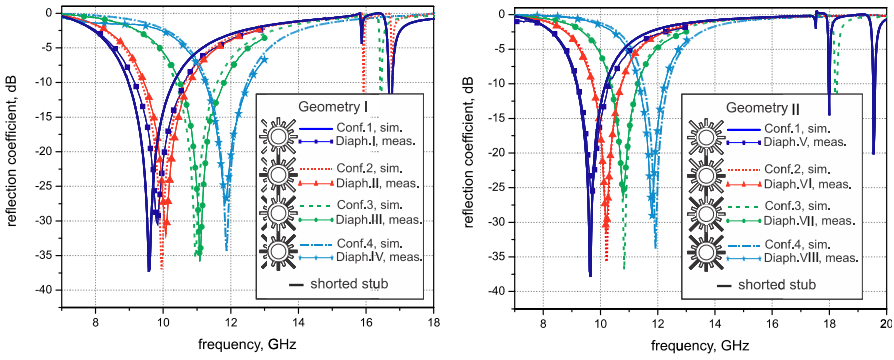

Figure 8. Comparison between measured reflection coefficient in the case of waveguide simulator and calculated reflection coefficient in the case of a RFSS with metal strips and open circuits instead of switching elements. (a) Geometry I. (b) Geometry II.

Table 1. Summary of measured and simulated results of the two geometries in the waveguide simulator.

				Resonant frequency (GHz)		Reflection coefficient at center frequency (dB)		-10 dB Reflection coefficient bandwidth (GHz)		Incident angle θ_0 at center frequency (°)
Geometry	Conf.	Diaph.	Switches in on-state	Simulated	Measured	Simulated	Measured	Simulated	Measured	Calculated
I	1	I	none	9.58	9.84	−37.34	−30.47	1.33	1.44	43.23
	2	II	1,3,5,7	9.95	10.08	−36.96	−31.88	1.30	1.34	41.26
	3	III	2,4,6,8	10.95	11.08	−35.34	−35.81	1.23	1.30	36.82
	4	IV	all	11.87	11.84	−34.32	−27.25	1.18	1.32	33.56
II	1	V	none	9.65	9.68	−37.84	−25.92	1.01	1.08	42.84
	2	VI	1,3,5,7	10.23	10.20	−35.69	−31.55	0.99	1.01	39.90
	3	VII	2,4,6,8	10.83	10.80	−36.93	−26.36	0.93	0.96	37.29
	4	VIII	all	11.93	11.80	−33.77	−29.26	0.86	0.90	33.37

5.2. Active Single Cell Element Diaphragms with MEMS Switches

Active diaphragms that contain one ring slot resonator with two horizontal switchable stubs were printed on a 0.2 mm-thick Rogers 4003 substrate using a standard photolithography etching process. The RMSW200^{TM} inline series type RF MEMS switch from RADANT® MEMS was used to toggle the stubs. The bias circuits were built by patterning islands of Benzocyclobutene (BCB) on top of the cooper base of the circuit. The 5 µm-thick BCB film, which

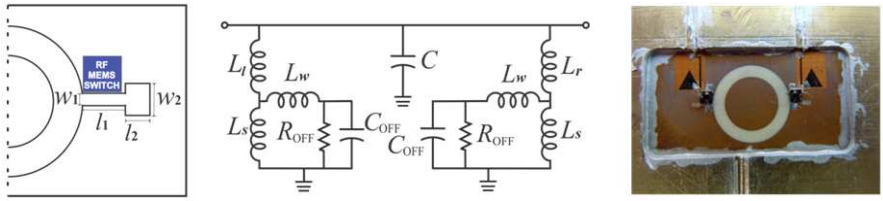

Figure 9. Active diaphragm with MEMS switches. (a) Half of the geometry of the unit cell with non-uniform stubs. (b) Equivalent circuit model. (c) Fabricated diaphragm installed in the waveguide.

acts as an insulator, has a 1 µm-thick cooper film deposited on top of it to form the DC bias lines [46]. To isolate the RF from the DC source, open ended stubs were patterned on the cooper film to form low-pass filters. To reduce the bond-wire parasitics, the stub geometry was modified as shown in Fig. 9(a). Thus, non-uniform stubs with two sections of lengths l_1 and l_2, and widths w_1 and w_2, were used to obtain shorter lengths of the wire. A 25-µm-diameter gold wire was bonded to make the interconnections between the bond pads of the RF MEMS switches and the metal part of the diaphragm. Additionally, a series inductance of L_w was added to the switch's model to take into account the bonded gold wires (Fig. 9(b)). To avoid any microwave power leakage, a conductive silver paste was used to seal the diaphragm's edges and to fill in the slots with bias lines. Then three diaphragms (IX, X, XI) with different ring slot widths were fabricated and tested. Diaphragm IX is given by: $r_1 = 3\,\text{mm}$, $r_2 = 3.5\,\text{mm}$, $l_1 = 1.62\,\text{mm}$, $l_2 = 0.73\,\text{mm}$, $w_1 = 0.2\,\text{mm}$, and $w_2 = 0.5\,\text{mm}$. Diaphragm X is defined by: $r_1 = 3.3\,\text{mm}$, $r_2 = 4.7\,\text{mm}$, $l_1 = 1.62\,\text{mm}$, $l_2 = 0.38\,\text{mm}$, $w_1 = 0.2\,\text{mm}$, and $w_2 = 0.5\,\text{mm}$. Diaphragm XI is set by: $r_1 = 3.25\,\text{mm}$, $r_2 = 5\,\text{mm}$, $l_1 = 1.62\,\text{mm}$, $l_2 = 0.31\,\text{mm}$, $w_1 = 0.2\,\text{mm}$, and $w_2 = 0.5\,\text{mm}$. These diaphragms were installed at the cross section of a rectangular waveguide WR-90 (Fig. 9(c)). DC bias voltages of 95 and 0 V were applied to the gate of the RF MEMS switches to set the on- and off-states, respectively.

Also, the mathematical model was used to obtain the parameters of the equivalent circuit of the off-state MEMS switch. As our model was not built for taking into account non-uniform stubs, the equivalent diaphragms with uniform stubs corresponding to Diaphragms IX, X and XI were used in the simulation. Then, the experimental data was approximated by the simulated curves shown in Fig. 10. As a result, Equivalent diaphragm IX is given by: $r_1 = 3\,\text{mm}$, $r_2 = 3.5\,\text{mm}$, $l_s =$

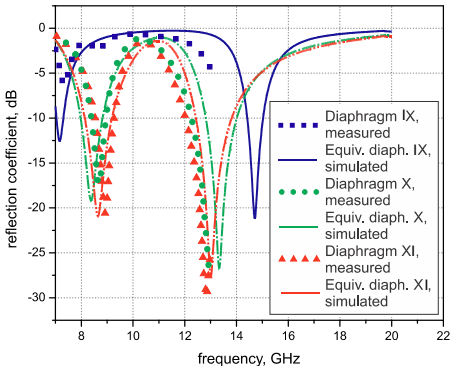

Figure 10. Simulated reflection coefficient of the equivalent diaphragms and measured reflection coefficients of the fabricated diaphragms.

4.2 mm, and $w = 0.2$ mm, Equivalent diaphragm X is defined by: $r_1 = 3.3$ mm, $r_2 = 4.7$ mm, $l_s = 3.1$ mm, and $w = 0.2$ mm, and Equivalent diaphragm XI is set by: $r_1 = 3.25$ mm, $r_2 = 5$ mm, $l_s = 2.9$ mm, and $w = 0.2$ mm. The three equivalent diaphragms have $b_x = 22.86$ mm and $b_y = 10.16$ mm. To obtain the parameters of the equivalent circuit of the off-sate MEMS, the measured results for each of the three fabricated diaphragms were approximated by the corresponding simulated curves calculated with the developed mathematical model that took into account the impedance $\bar{Z}_k$ of the off-state equivalent circuit. As a result, for all three fabricated diaphragms, the parameters of the equivalent circuit of the off-state MEMS switch were found as: $C_{\text{OFF}} = 0.08$ pF and $R_{\text{OFF}} = 3.4\,\text{k}\Omega$. The bond wire inductance was $L_w = 0.86$ nH. Fig. 10 shows the comparison between the measured reflection coefficients of the fabricated diaphragms installed into the WR-90 waveguide and the simulated reflection coefficients of the equivalent diaphragms.

The analysis of the obtained results demonstrates that ring slots with smaller slot widths are less sensitive to the effects of the switch's off-state capacitance. A smaller slot width produces a higher electric field in the ring slot, forming a large capacitance. Therefore, when the parasitic capacitance of the switch interacts with the large slot's capacitance, the switch's capacitance has less impact on the RFSS element's performance. For a smaller slot width, a smaller frequency shift in the main resonance, as well as a secondary resonance occurring at a higher frequency and resulting in a larger upper stop band are observed.

6. CONCLUSION

A novel RFSS element based on ring slot resonators loaded with switchable radial stubs has been proposed, fabricated, and tested. The element has the potential to set various resonant transmission frequencies according to the on-off combination of the switches. Also, the proper on-off combination of the switches can ensure polarization diversity. An equivalent circuit model and a full-wave mathematical model were built to analyze the reflection characteristics of the infinite RFSS. As a result, a RFSS for X band operation was designed with resonant frequencies at 9.65, 10.28, 10.83 and 12.05 GHz. Parasitic effects of the off-state RF MEMS switches were also analyzed. Although these parasitic effects at microwave frequencies result in the onset of unwanted higher order resonances, proper geometry optimization of the RFSS element can diminish or allocate to upper frequencies these unwanted effects. Furthermore, off-state switch's capacitance can extend the reconfigurability range. The use of commercially available RF MEMS switches in RFSS elements was also proved. The described element presented here is suitable for low-loss and low-power consumption RFSS applications.

ACKNOWLEDGMENT

This work was partially supported by Research Grants PAPIIT IN114911, PAPIIT IN116112, and CONACYT 166106. The authors would like to thank D. T. Mendoza-Rosales for his assistance in the photolithography process.

REFERENCES

1. Munk, B. A., *Frequency Selective Surfaces: Theory and Design*, Wiley-Interscience, New York, 2000.
2. Wu, T. K., *Frequency Selective Surfaces and Grid Arrays*, Wiley, New York, 1995.
3. Monni, S., A. Neto, G. Gerini, F. Nennie, and A. Tijhuis, "Frequency-selective surface to prevent interference between radar and SATCOM antennas," *IEEE Antennas Wireless Propag. Lett.*, Vol. 8, 220–223, 2009.
4. Erdemli, Y. E., K. Sertel, R. A. Gilbert, D. E. Wright, and J. L. Volakis, "Frequency-selective surfaces to enhance performance of broad-band reconfigurable arrays," *IEEE Trans. on Antennas and Propag.*, Vol. 50, No. 12, 1716–1724, 2002.

5. Wu, B.-I., W. Wang, J. Pacheco, X. Chen, T. M. Grzegorczyk, and J. A. Kong, "A study of using metamaterials as antenna substrate to enhance gain," *Progress In Electromagnetics Research*, Vol. 51, 295–328, 2005.
6. Chen Y., S. Yang, and Z.-P. Nie, "A novel wideband antenna array with tightly coupled octagonal ring elements," *Progress In Electromagnetics Research*, Vol. 124, 55–70, 2012.
7. Sung G. H., K. W. Sowerby, and A. G. Williamson, "Modeling a low-cost frequency selective wall for wireless-friendly indoor environments," *IEEE Antennas Wireless Propag. Lett.*, Vol. 5, 311, 2006.
8. Barlevy, A. S. and Y. Rahmat-Samii, "On the electrical and numerical properties of high Q resonances in frequency selective surface," *Progress In Electromagnetics Research*, Vol. 22, 1–27, 1999.
9. Feresidis, A. P., G. Goussetis, S. Wang, and J. C. Vardaxoglou, "Artificial magnetic conductor surfaces and their application to low-profile high-gain planar antennas," *IEEE Trans. on Antennas and Propag.*, Vol. 53, No. 1, 209–215, 2005.
10. Sohn, J. R., K. Y. Kim, H.-S. Tae, and H. J. Lee, "Comparative study on various artificial magnetic conductors for low-profile antenna," *Progress In Electromagnetics Research*, Vol. 61, 27–37, 2006.
11. Kim, Y., F. Yang, and A. Z. Elsherbeni, "Compact artificial magnetic conductor designs using planar square spiral geometries," *Progress In Electromagnetics Research*, Vol. 77, 43–54, 2007.
12. De Cos, M. E., Y. Alvarez Lopez, R. C. Hadarig, and F. Las-Heras, "Flexible uniplanar artificial magnetic conductor," *Progress In Electromagnetics Research*, Vol. 106, 349–362, 2010.
13. Pirhadi, A., M. Hakkak, and F. Keshmiri, "Using electromagnetic bandgap superstrate to enhance the bandwidth of probe-fed microstrip antenna," *Progress In Electromagnetics Research*, Vol. 61, 215–230, 2006.
14. Cheype, C., C. Serier, M. Thevenot, T. Monediere, A. Reineix, and B. Jecko, "An electromagnetic bandgap resonator antenna," *IEEE Trans. on Antennas and Propag.*, Vol. 50, No. 9, 1285–1290, 2002.
15. Lee, D. H., Y. J. Lee, J. Yeo, R. Mittra, and W. S. Park, "Design of novel thin frequency selective surface superstrates for dual-band directivity enhancement," *IET Microwaves, Antennas Propag.*, Vol. 1, No. 1, 248–254, 2007.

16. Wu, B.-I., W. Wang, J. Pacheco, X. Chen, T. M. Grzegorczyk, and J. A. Kong, "A study of using metamaterials as antenna substrate to enhance gain," *Progress In Electromagnetics Research*, Vol. 51, 295–328, 2005.
17. Raspopoulos, M. and S. Stavrou, "Frequency selective buildings through frequency selective surfaces," *IEEE Trans. on Antennas and Propag.*, Vol. 59, No. 8, 2998–3005, 2011.
18. Chang, T. K., R. J. Langley, and E. A. Parker, "Active frequency-selective surfaces," *IEE Proceedings — Microwaves, Antennas and Propagation*, Vol. 143, No. 1, 62–66, 1996.
19. Kiani, G. I., K. L.Ford, L. G. Olsson, K. P. Esselle, and C. J. Panagamuwa, "Switchable frequency selective surface for reconfigurable electromagnetic architecture of buildings," *IEEE Trans. on Antennas and Propag.*, Vol. 58, No. 2, 581–584, 2010.
20. Chang, K., J. Langley, and E. Parker, "Frequency selective surfaces on biased ferrite substrates," *Electron. Lett.*, Vol. 30, No. 5, 1193–1194, 1994.
21. Zhang, J.-C., Y.-Z. Yin, and R. Yi, "Resonant characteristics of frequency selective surfaces on ferrite substrates," *Progress In Electromagnetics Research*, Vol. 95, 355–364, 2009.
22. Lima, A. C., E. A. Parker, and R. J. Langley, "Tunable frequency selective surface using liquid substrates," *Electron. Lett.*, Vol. 30, 281, 1994.
23. Simms, R. J. T., R. Dickie, R. Cahill, N. Mitchell, H. Gamble, and V. Fusco, "Measurement of electromagnetic properties of liquid crystals at 300 GHz using a tunable FSS," *31st ESA Workshop on Antennas for Space Applications, European Space Agency*, Holland, Oct. 2010
24. Zendejas, J. M., J. P. Gianvittorio, Y. Rahmat-Samii, and J. W. Judy, "Magnetic MEMS reconfigurable frequency-selective surfaces," *J. Microelectromech. Syst.*, Vol. 15, No. 3, 613–623, 2006.
25. Martynyuk, A. E., J. I. Martinez-Lopez, and N. A. Martynyuk, "Active frequency selective surfaces based on loaded ring slot resonators," *Electron. Lett.*, Vol. 41, No. 1, 2–4, 2005.
26. Malyuskin, O., V. F. Fusco, and A. G. Schuchinsky, "Modelling of impedance loaded wire frequency selective surfaces with tunable reflection and transmission characteristics," *International Journal of Numerical Modeling: Electronic Networks, Devices and Fields*, Vol. 21, No. 6, 439–453, 2008.

27. Sanz-Izquierdo, B., E. A. Parker, and J. C. Batchelor, "Switchable frequency selective slot arrays," *IEEE Trans. on Antennas and Propag.*, Vol. 59, No. 7, 2728–2731, 2011.
28. Mias C., "Varactor-tunable frequency selective surface with resistive-lumped-element biasing grids," *IEEE Microw. Wireless Compon. Lett.*, Vol. 15, 570–572, 2005.
29. Durbin, J. L. and M. A. Saed, "Tunable filtenna using varactor tuned rings FED with an ultra wideband antenna," *Progress In Electromagnetics Research Letters*, Vol. 29, 43–50, 2012.
30. Costa, F., A. Monorchio, S. Talrico, and F. M. Valeri, "An active high-impedance surface for low-profile tunable and steerable antennas," *IEEE Antennas Wireless Propag. Lett.*, Vol. 7, 676–680, 2008.
31. Schoenlinner, B., A. Abbaspour-Tamijani, L. C. Kempel, and G. M. Rebeiz, "Switchable low-loss RF MEMS ka-band frequency-selective surface," *IEEE Trans. on Microw. Theory and Tech.*, Vol. 52, No. 11, 2474–2481, 2004.
32. Coutts, G. M., R. R. Mansour, and S. K. Chaudhuri, "Microelectromechanical systems tunable frequency-selective surfaces and electromagnetic-bandgap structures on rigid-flex substrates," *IEEE Trans. on Microw. Theory and Tech.*, Vol. 56, No. 7, 1737–1746, 2008.
33. Radi, Y., S. Nikmehr, and A. Poorziad, "A novel bandwidth enhancement technique for x-band RF Mems actuated reconfigurable reflectarray," *Progress In Electromagnetics Research*, Vol. 111, 179–196, 2011.
34. Tahir, F. A., H. Aubert, and E. Girard, "Equivalent electrical circuit for designing mems-controlled reflectarray phase shifters," *Progress In Electromagnetics Research*, Vol. 100, 1–12, 2010.
35. Parker, E. A. and S. M. A. Hamdy, "Rings as elements for frequency selective surfaces," *Electron. Lett.*, Vol. 17, No. 17, 612–614, Aug. 20, 1981.
36. Martynyuk, A. E. and J. I. Martinez-Lopez, "Frequency-selective surfaces based on shorted ring slots," *Electron. Lett.*, Vol. 37, No. 5, 268–269, Mar. 1, 2001.
37. Taylor, P. S., E. A. Parker, and J. C. Batchelor, "An active annular ring frequency selective surface," *IEEE Trans. on Antennas and Propag.*, Vol. 59, No. 9, 3265–3271, 2011.
38. Ucar, M. H. B., A. Sondas, and Y. E. Erdemli, "Switchable split-ring frequency selective surfaces," *Progress In Electromagnetics Research B*, Vol. 6, 65–79, 2008.

39. Taylor, P. S., J. C. Batchelor, and E.A. Parker, "Dual-band FSS design using LC traps," *Antennas and Propagation Conference (LAPC)*, 405–408, Loughborough, Nov. 8–9, 2010.
40. Kondo, A., "Design and characteristics of ring-slot type FSS," *Electron. Lett.*, Vol. 27, No. 3, 240–241, 1991.
41. Harrington, R. F., "The method of moments in electromagnetics," *Journal of Electromagnetic Waves and Applications*, Vol. 1, No. 3, 181–200, 1987.
42. Amitay, N., V. Galindo, and C. P. Wu, *Theory and Analysis of Phased Array Antennas*, Wiley-Interscience, New York, 1972.
43. Chen, C.-C., "Transmission through a conducting screen perforated periodically with apertures," *IEEE Trans. on Microw. Theory and Tech.*, Vol. 18, No. 9, 627–632, 1970.
44. Vendik I. B., O. G. Vendik, and E. L. Kollberg, "Commutation quality factor of two-state switchable devices," *IEEE Trans. on Microw. Theory and Tech.*, Vol. 48, No. 5, 802–808, May 2000.
45. Martynyuk, A. E., A. G. Martinez-Lopez, and J. Rodriguez-Cuevas, "Spiraphase-type element with optimal transformation of switch impedances," *Electron. Lett.*, Vol. 46, No. 10, 673–675, 2010.
46. Martynyuk, A. E., A. G. Martinez-Lopez, and J. I. Martinez-Lopez, "2 bit X-band reflective waveguide phase shifter with BCB based bias circuits," *IEEE Trans. on Microw. Theory and Tech.*, Vol. 54, No. 12, 4056–4061, 2006